rnational Journal Of Innovative Trends In Multi Disciplinary Scientific Research
ISSN (Online): 3139 – 2687
(www.ijtmsr.co.in) Volume 9, Issue 8, 2026

Structural and Modal Performance Optimization of a Vertical Axis Wind Turbine Blade Using Analytical and Finite Element Methods

M.RAJASEKHAR[1], V.NAGA BHUSHAN RAO[2]

[1]PG scholar, Department of Mechanical engineering, Raghu Engineering College (A), Visakhapatnam.

[2] Professor, Department of Mechanical engineering, Raghu Engineering College (A), Visakhapatnam..

ABSTRACT

This paper investigates the structural and dynamic performance of a NACA 0015 straight-bladed vertical axis wind turbine (VAWT) blade using analytical beam theory and finite element analysis (FEA) in ANSYS Workbench. The 2.58 m blade with a 206.2 mm chord is supported at two locations positioned 0.56 m from the free ends. Six cross-sectional configurations (solid, 5, 4, 3, 2 and 1 mm wall thickness) and six materials (Aluminum, Kevlar 149, Technora, Glass E, Glass S and Graphite Epoxy) are compared. Static analysis evaluates deflection and bending stress, while modal analysis determines the first three natural frequencies. The analytical and numerical predictions show consistent trends, with FEM values generally slightly higher because of its more detailed representation of local bending and support effects. Thickness reduction decreases self-weight and loading and improves the response until the loss of sectional stiffness becomes significant. The analytical results identify approximately 2 mm as the minimum-deflection/stress region, whereas the FEM results often continue to show low deflection at 1–2 mm. Kevlar 149 provides the strongest overall stiffness-to-weight response among the adopted material models. The study demonstrates that a thin-walled high-stiffness composite blade can provide a structurally efficient VAWT configuration when static and vibration requirements are considered together.

Keywords: *Vertical axis wind turbine; NACA 0015; finite element analysis; ANSYS Workbench; modal analysis; wall thickness; composite materials; beam theory.*

I. INTRODUCTION

Wind energy is an important renewable-energy technology because it converts the kinetic energy of moving air into useful mechanical and electrical energy without fuel consumption during operation. Vertical axis wind turbines are particularly attractive for locations with changing wind direction because the rotor can accept wind from different horizontal directions without continuous yaw control. However, VAWT blades experience continuously varying aerodynamic forces during rotation, producing repeated bending, deformation and vibration. Structural integrity and dynamic stability are therefore essential design requirements in addition to aerodynamic efficiency.



Fig 1 Vertical axis wind turbine .

A lightweight blade is desirable because reduced rotating mass can lower inertial and centrifugal effects, but excessive thickness reduction decreases bending rigidity and can increase deformation or stress. Material selection introduces a second design variable because density and Young's modulus govern the mass–stiffness relationship. This study therefore compares metallic, aramid, glass and graphite-based material models over a systematic thickness range. The objective is to identify a lightweight configuration that maintains favorable static and modal performance using a common geometry, loading and support arrangement.

II. LITERATURE REVIEW

Recent VAWT studies increasingly combine structural FEA, composite-material design, modal assessment and lightweight optimization. Seralathan et al. [1] demonstrated through static analysis that changes in material stiffness and density significantly affect deformation and stress under common geometry and loading. Öğüçlü [2] investigated a helical VAWT blade and emphasized the need to evaluate material strength against wind-induced structural demand. Hand et al. [3] compared analytical and detailed FE models for an offshore composite VAWT blade and reported useful agreement between the two approaches, supporting analytical–numerical validation strategies.

Carnevale et al. [4] showed that non-stationary operating events can generate important stress cycles in VAWTs, highlighting the relevance of structural dynamics and fatigue. Nachtane et al. [5] examined offshore Darrieus-type concepts and reinforced the importance of material and section configuration under severe loading. Boudounit et al. [6] linked finite-element stress fields with fatigue analysis for composite wind-turbine blades. Akimoto et al. [7] used parametric FEA and genetic optimization to minimize VAWT structural mass while satisfying design constraints, demonstrating the advantage of optimizing material and geometry simultaneously.

Nezzar et al. [8] compared aluminum and glass/epoxy blade concepts and showed that composite design can substantially

rnational Journal Of Innovative Trends In Multi Disciplinary Scientific Research
ISSN (Online): 3139 – 2687
(www.ijtmsr.co.in) Volume 9, Issue 8, 2026

reduce mass while maintaining acceptable deformation and stress. Mishnaevsky et al. [9] reviewed wind-turbine blade materials and identified specific stiffness, strength, damage tolerance and fatigue resistance as major selection criteria. Jensen and Branner [10] emphasized the interaction between composite material distribution and cross-sectional stiffness. Lagdani et al. [11] demonstrated that changes in mass distribution modify blade natural frequencies, while Jayswal and Bhattu [12] directly connected material choice with static and modal performance.

More recent work has treated fatigue and dynamic response as integrated design requirements. Nijssen and Brøndsted [13] discussed fatigue as a major design driver for composite blades, and Ghoneam et al. [14] combined modal analysis, fatigue-life estimation and multi-response optimization for VAWT composites. Hardt et al. [15] showed that cross-sectional modelling strongly influences predicted stiffness and optimization outcomes. These studies establish the need to evaluate thickness and material together rather than independently.

Most reported investigations consider one or two blade materials, a limited set of laminate arrangements, or a single optimized section. A direct comparison of Aluminum, Kevlar 149, Technora, Glass E, Glass S and Graphite Epoxy using the same NACA 0015 blade, identical supports, and a solid-to-1 mm thickness sequence is limited. The present work addresses this gap through a consistent analytical and ANSYS-based structural and modal comparison.

III. MATERIALS AND METHODS

The vertical axis wind turbine blade considered in this study is a straight-bladed Darrieus configuration designed using a symmetric NACA 0015 airfoil. Symmetric airfoils are suitable for VAWTs because the blade experiences continuously changing relative wind directions during each revolution and must maintain comparable aerodynamic behaviour at positive and negative angles of attack. Among NACA 0012, NACA 0015 and NACA 0018, the NACA 0015 profile was selected as a suitable compromise between aerodynamic performance and structural thickness.

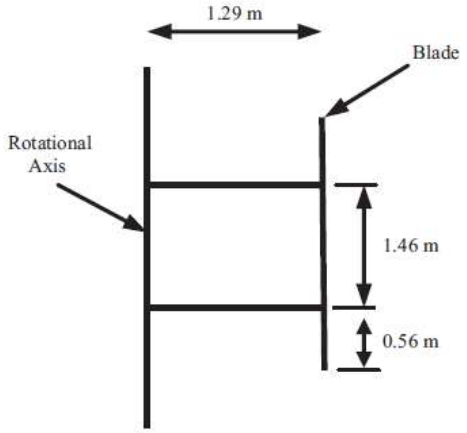


Fig 2 Blade Supports.

The blade is subjected to varying lift and drag forces during rotation, and the maximum normal aerodynamic force of 681 N is adopted as the principal design load for structural calculations. The blade is supported at two strut locations, leaving approximately 0.56 m cantilever portions at both ends and a central span of about 1.46 m. This support arrangement reduces the effective unsupported length and helps control bending stress and deformation while maintaining the same boundary condition for all design cases.

To evaluate the influence of cross-sectional geometry, the NACA 0015 blade is investigated using a solid section and hollow sections of 5 mm, 4 mm, 3 mm, 2 mm and 1 mm wall thickness. The solid blade serves as the reference configuration, while progressive reduction in wall thickness decreases material volume, structural mass and centrifugal loading. However, reducing thickness also changes the second moment of area, bending stiffness and torsional rigidity, making it necessary to evaluate deformation, stress, modal response and fatigue characteristics before selecting an optimum section. The blade experiences both aerodynamic and centrifugal loading during operation, and centrifugal force is strongly dependent on blade mass and rotational speed.

A. BLADE GEOMETRY AND MATERIAL PROPERTIES

Parameter	Value
Blade length	2.58 m
Chord length	206.2 mm
Airfoil	NACA 0015
Support positions	0.56 m from each free end
Central span	1.46 m
Cross-sections	Solid, 5, 4, 3, 2, 1 mm
Design normal force	681 N
FE mesh	50 beam elements

Table 1 Geometry parameters.

Six material models were assigned under identical geometry and boundary conditions. Their adopted elastic modulus and density values are summarized in Table 2. The graphite modulus of 27.6 GPa is retained exactly as used in the project model, which explains its comparatively flexible response.

Material	Elastic Modulus, E (GPa)	Density (kg/m³)
Aluminum	70	2700
Kevlar 149	179	1470
Technora	70	1390
Glass E	76	2540
Glass S	88	2540
Graphite	27.6	1800

Table 2. Material properties adopted in the numerical model.

rnational Journal Of Innovative Trends In Multi Disciplinary Scientific Research
ISSN (Online): 3139 – 2687
(www.ijtmsr.co.in) Volume 9, Issue 8, 2026

B. ANALYTICAL STRUCTURAL MODEL

Fixed Region (Uniformly Distributed Load on a fixed-fixed / simply supported span)

Reaction force, $R = V = WL / 2$

Bending moment at end, $M_{enx} = WL^2 / 12$

Bending moment at center, $M_{eenter} = WL^2 / 24$

Deflection at center, $\delta = WL^4 / (384\ EI)$

Maximum stress, $\sigma = WL / (12\ Z)$

Cantilever Region (Uniformly Distributed Load on a cantilever span)

Maximum bending moment, $M_{max} = WL^2 / 2$

Maximum deflection, $\delta_{max} = WL^4 / (8\ EI)$

Maximum stress, $\sigma = WL / (2\ Z)$

Where W = distributed load intensity (UDL, from the base paper), L = span length, E = modulus of elasticity (70 GPa), I = second moment of area (Ixx) of the section, and Z = section modulus.

Fixed Region (Span L = 1.46 m)

Case 1: Solid Section

$R = V = (10.08 \times 10^3 \times 1.46) / 2 = 7358.4$ N

Bending moment at end $= (10.08 \times 10^3 \times 1.46^2) / 12 = 1.79054$ kN·m

Bending moment at center $= (10.08 \times 10^3 \times 1.46^2) / 24 = 895.272$ N·m

Deflection at center $= (10.08 \times 1.46^4) / (384 \times 70 \times 10^9 \times 2.04 \times 10^{-7}) = 7.09$ mm

Max. stress $= (10.08 \times 10^3 \times 1.46) / (12 \times 1.0572 \times 10^{-5}) = 116{,}004{,}540.3$ N/m² = 116.0045 MPa

Force = UDL × L = 10.08 × 1.46 = 14.71 kN

Case / Wall Thickness	UDL (kN/m)	Reaction / Force (kN)	B.M. at End (kN·m)	Deflection at Center (mm)	Max. Stress (MPa)
Solid	10.08	14.71	1.7905	7.09	116.00
5 mm	4.59	6.7014	0.815	4.33	70.51
4 mm	3.78	5.518	0.671	4.10	66.80
3 mm	2.94	4.29	0.522	3.91	63.60
2 mm	2.08	3.036	0.369	3.82	62.10
1 mm	1.16	1.693	0.205	3.92	65.21

Table 3 Summary Table for Fixed Region

Table 3 presents the calculated loading and structural response of the cantilever region for the solid and different wall-thickness configurations. The solid section experiences the highest uniformly distributed load (UDL) of 10.08 kN/m, corresponding to a force of 14.71 kN and an end bending moment of 1.7905 kN·m. As the wall thickness is reduced, the structural weight and associated loading decrease considerably, with the 1 mm section producing only 1.16 kN/m UDL, 1.693 kN force, and 0.205 kN·m bending moment. The deflection decreases from 7.09 mm for the solid section to a minimum of 3.82 mm at 2 mm thickness, before slightly increasing to 3.92 mm at 1 mm. A similar trend occurs in maximum stress, which decreases from 116 MPa for the solid section to 62.10 MPa at 2 mm, followed by an increase to 65.21 MPa at 1 mm. This indicates that reducing thickness initially provides a significant benefit because the reduction in self-weight and bending load exceeds the loss in sectional stiffness. However, at 1 mm, the section becomes sufficiently thin that the reduction in moment of inertia begins to dominate, causing deformation and stress to rise. Among the investigated hollow configurations, the 2 mm section therefore provides the lowest calculated deformation and stress in the cantilever region.the same calculation is done for remaining materials.

C. MODAL ANALYSIS CALCULATIONS

Modal analysis is carried out to determine the natural frequencies and corresponding mode shapes of the blade. For a simplified single-degree representation, natural frequency is proportional to the square root of the ratio of structural stiffness to mass, $f \propto \sqrt{(k/m)}$. For a beam, stiffness depends strongly on the product EI, while mass per unit length depends on density and cross-sectional area. Consequently, changing material from aluminum to Kevlar, Technora, glass or graphite changes both stiffness and mass, and reducing wall thickness changes both section rigidity and mass. The resulting natural-frequency trend therefore cannot be predicted from density alone.

The modal results are used to identify whether any blade configuration has relatively low natural frequencies that could approach operational excitation frequencies. The associated mode shapes indicate whether the blade response is dominated by bending, torsion or a more complex deformation pattern. A suitable blade configuration should maintain adequate separation between its important natural frequencies and the principal rotational or aerodynamic excitation frequencies. This dynamic requirement is considered together with the static structural results when identifying an appropriate material and thickness.

$f_n = (\beta_n L)^2 / (2\pi L^2) \times \sqrt{(EI / \rho A)}$,

with the fixed–fixed boundary-condition constants $\beta_n L$ = 4.730, 7.853, 10.996 for the fixed region (L = 1.46 m), and the cantilever (fixed–free) constants $\beta_n L$ = 1.875, 4.694, 7.855 for the cantilever region (L = 0.56 m).

Aluminum — Calculation

E = 70 GPa, $\rho = 2700$ kg/m³.

Fixed Region (L = 1.46 m)

Mode constants = $\beta_1 L = 4.730$, $\beta_2 L = 7.853$, $\beta_3 L = 10.996$

$f_1 = (4.730)^2 / (2\pi \times 1.46^2) \times \sqrt{(70 \times 10^9 \times 2.04 \times 10^{-7} / (2700 \times 1.1698 \times 10^{-3}))} = 112.32$ Hz

rnational Journal Of Innovative Trends In Multi Disciplinary Scientific Research
ISSN (Online): 3139 – 2687
(www.ijtmsr.co.in) Volume 9, Issue 8, 2026

Case / Wall Thickness	Outer D (mm)	Area A (mm²)	f_1 (Hz)	f_2 (Hz)	f_3 (Hz)
Solid	38.59	1169.76	112.32	309.61	607.04
5 mm	45.20	631.49	143.20	394.73	773.92
4 mm	45.32	519.22	147.43	406.39	796.78
3 mm	45.20	397.69	152.00	418.97	821.45
2 mm	45.15	271.14	156.68	431.87	846.74
1 mm	46.11	141.70	159.61	439.96	862.60

Table 4 Aluminum Fixed region frequency results.

The table shows that the natural frequencies of the aluminum blade in the fixed region increase progressively as the wall thickness is reduced. The first natural frequency increases from 112.32 Hz for the solid section to 159.61 Hz for the 1 mm section, while the second frequency increases from 309.61 Hz to 439.96 Hz and the third frequency from 607.04 Hz to 862.60 Hz. Although the cross-sectional area decreases considerably from 1169.76 mm² to 141.70 mm², the corresponding change in the relationship between bending stiffness and mass results in higher calculated natural frequencies. Among the investigated aluminum configurations, the 1 mm section produces the highest frequencies in all three modes, whereas the solid section produces the lowest.the same calculation are done for remaining materials.

D. FINITE ELEMENT AND MODAL ANALYSIS

The CATIA blade was imported into ANSYS SpaceClaim and converted from the three-dimensional geometry to a NACA 0015 beam cross-section and longitudinal line body. The line was split at the two support locations, 0.56 m from each free end. This produced two cantilever segments and a 1.46 m central region consistent with the analytical model. The beam representation retained the cross-sectional properties required for bending and vibration while reducing computational cost.

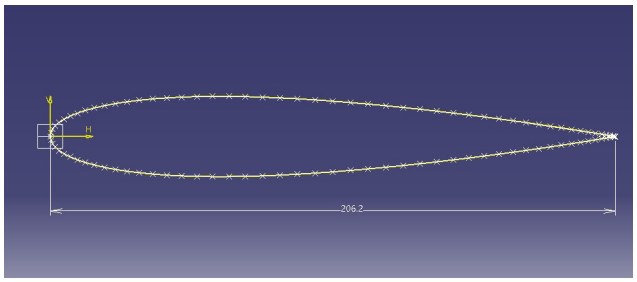


Figure 2. NACA 0015 airfoil profile used for the blade model.

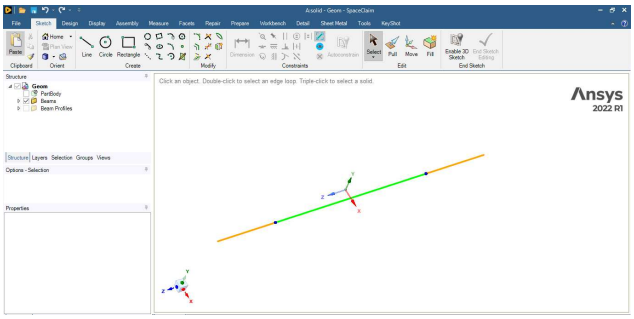


Figure 3. Beam-line finite element model and mesh of the VAWT blade.

The complete 2.58 m line body was discretized with 50 beam elements. Fixed supports constrained all translational and rotational degrees of freedom at the two strut locations. In the static structural analysis, the calculated uniformly distributed loads were applied to the corresponding beam segments using line pressure. Total deformation, bending stress and bending moment were obtained from the solution. The same modelling procedure was repeated for all thicknesses and materials so that only the intended design variables changed.

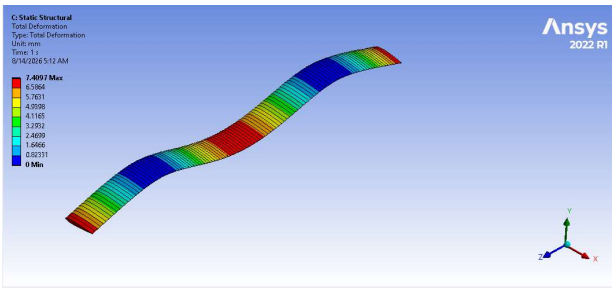


Fig 4: Displacement at solid blade.

Figure 4. shows the displacement distribution for the solid blade. The maximum displacement was 7.4 mm at the free cantilever ends, decreasing toward the fixed-support locations.

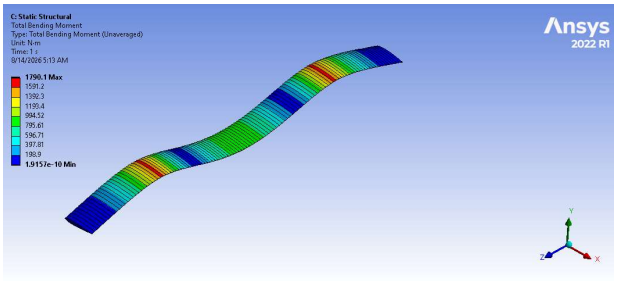


Fig 5: Bending moment at solid blade.

Figure 5 presents the bending-moment distribution. The maximum was 1.79 kN·m at the support locations, consistent with the fixed boundary conditions.

rnational Journal Of Innovative Trends In Multi Disciplinary Scientific Research
ISSN (Online): 3139 – 2687
(www.ijtmsr.co.in) Volume 9, Issue 8, 2026

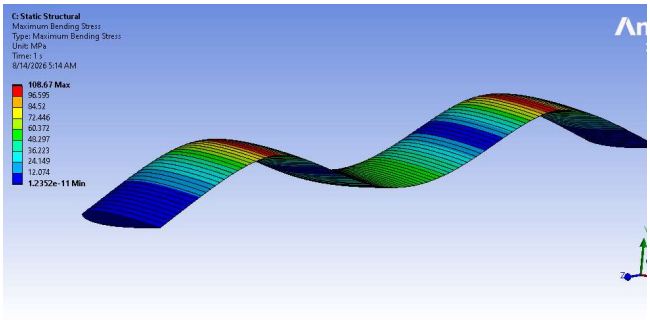


Fig 6: Bending stress at solid blade.

Figure 6 shows the corresponding bending stress, with a maximum of 108.6 MPa at the supports — the critical structural region under this loading.

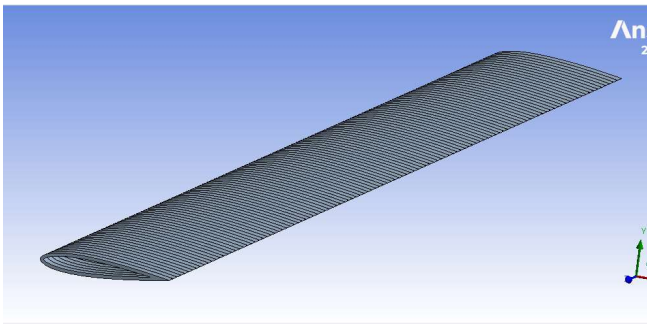


Fig 7: Geometry model of 5 mm thicked VAWT blade.

A 5 mm wall-thickness blade was next developed by applying a 5 mm offset to the NACA 0015 profile in CATIA and extruding the hollow geometry, then analyzed in ANSYS using the same methodology as the solid blade.

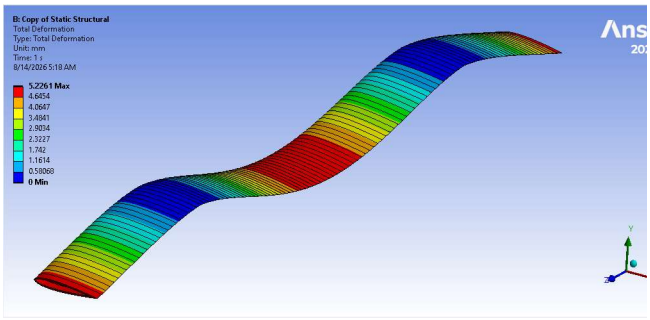


Fig 8: Displacement at 5 mm thicked blade.

Figure 8 shows a maximum displacement of 5.22 mm at the free cantilever ends — the same pattern as the solid blade, with reduced magnitude from the modified cross-section and loading.

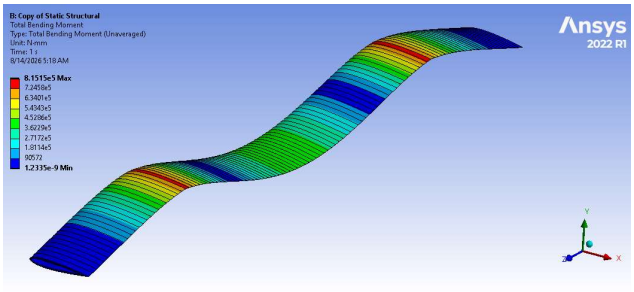


Fig 9: Bending moment at 5 mm ticked blade.

Figure 9 shows a maximum bending moment of 0.81 kN·m at the supports, lower than the solid blade due to the reduced hollow-section loading.

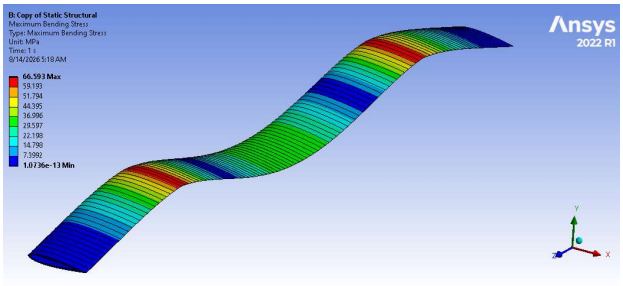


Fig 10: Bending stress at 5 mm ticked blade.

Figure 10 shows a maximum bending stress of 66.5 MPa at the supports, confirming these connections as the critical regions under bending.

The same FEM methodology — geometry, beam conversion, meshing, supports, and distributed loading via the Pressure on Line command — was then repeated for the 4, 3, 2 and 1 mm configurations, giving a consistent basis for comparing displacement, bending moment and bending stress across all wall thicknesses.

F. MODAL ANALYSIS

Modal analysis used the same geometry, material assignment, mesh and support locations, but the static UDL was not applied. ANSYS solved the undamped eigenvalue problem $([K] - \omega n^2[M])\{\phi n\} = 0$, and the natural frequency was calculated from $fn = \omega n/(2\pi)$. Analytical modal frequencies were estimated from Euler–Bernoulli beam theory: $fn = (\beta nL)^2/(2\pi L^2)\sqrt{(EI/\rho A)}$, using boundary-condition-specific β values. The first three modes were extracted for each configuration and compared with analytical predictions.

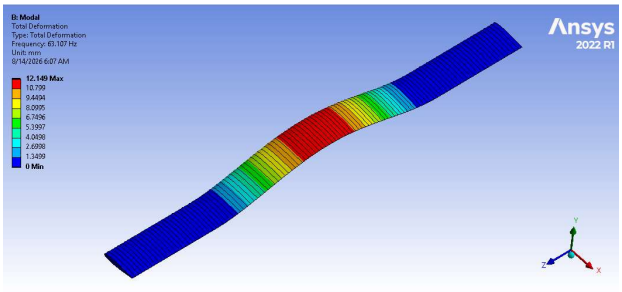


Fig 11: 1st mode of solid blade for aluminum.

Figure 11 presents the first vibration mode of the solid aluminum blade: a natural frequency of 63.1 Hz with a maximum modal displacement of 12.1 mm at the centre of the span between supports, approaching zero at the constrained ends.

G. VALIDATION STRATEGY

Validation was performed by comparing analytical beam-theory results with ANSYS predictions for deformation, bending stress and natural frequency. Percentage deviations were used as a consistency check. The analytical model provides a transparent first estimate, while FEA captures the

rnational Journal Of Innovative Trends In Multi Disciplinary Scientific Research
ISSN (Online): 3139 – 2687
(www.ijtmsr.co.in) Volume 9, Issue 8, 2026

discretized support and local bending behaviour in greater detail.

IV. Results and Discussion

A. STATIC STRUCTURAL ANALYSIS RESULTS

The static structural analysis evaluates the maximum deflection produced in each blade configuration under its self-weight/aerodynamic distributed loading, together with the resulting bending stress for the Aluminum blade. In each table the analytical (beam-theory) result is compared directly against the ANSYS finite element result for the same cross-section, and the accompanying graph plots both sets of values against blade thickness so that the trend with reducing wall thickness can be seen at a glance.

Aluminum

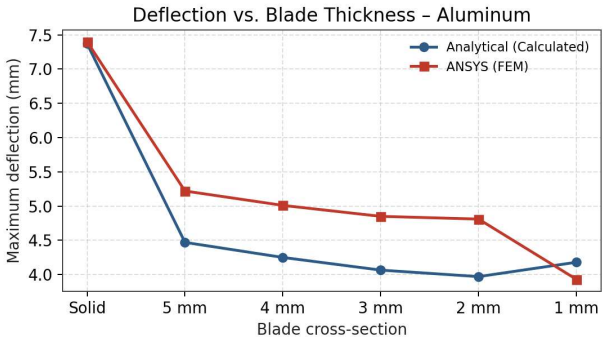


Fig 11 Deflection versus blade thickness, Aluminum.

ANSYS deflection falls to a minimum of 3.93 mm at 1 mm (46.9% reduction); the analytical minimum of 3.970 mm occurs at 2 mm before rising to 4.18 mm at 1 mm, with an average deviation of 13.6% between methods.

Kevlar

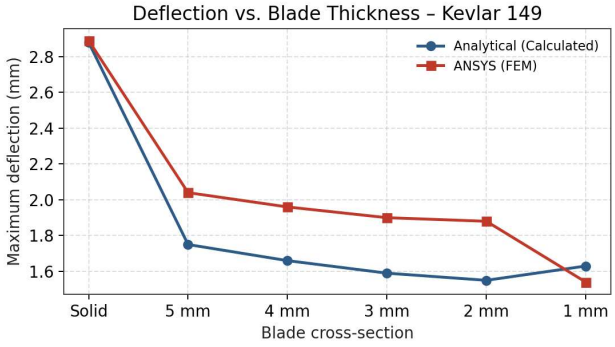


Fig 12 Deflection versus blade thickness, Kevlar 149.

ANSYS deflection falls to a minimum of 1.54 mm at 1 mm (46.7% reduction); the analytical minimum of 1.550 mm occurs at 2 mm before rising to 1.63 mm at 1 mm, with an average deviation of 13.5% between methods.

Technora

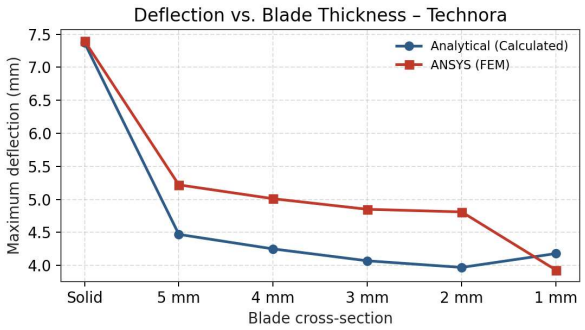


Fig 13 Deflection versus blade thickness, Technora.

ANSYS deflection falls to a minimum of 3.93 mm at 1 mm (46.9% reduction); the analytical minimum of 3.970 mm occurs at 2 mm before rising to 4.18 mm at 1 mm, with an average deviation of 13.6% between methods.

Glass E

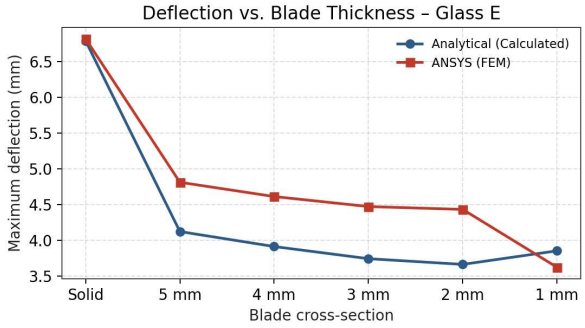


Fig 14 Deflection versus blade thickness, Glass E.

ANSYS deflection falls to a minimum of 3.62 mm at 1 mm (46.9% reduction); the analytical minimum of 3.660 mm occurs at 2 mm before rising to 3.85 mm at 1 mm, with an average deviation of 13.6% between methods.

Glass S

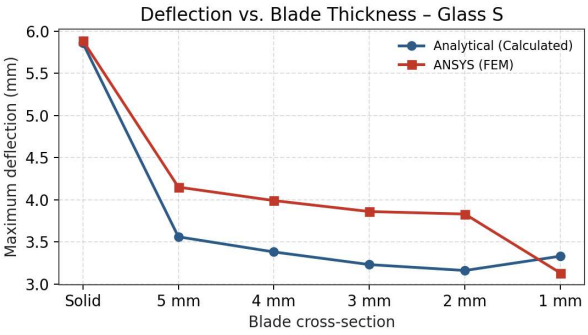


Fig 15 Deflection versus blade thickness, Glass S.

ANSYS deflection falls to a minimum of 3.13 mm at 1 mm (46.9% reduction); the analytical minimum of 3.160 mm occurs at 2 mm before rising to 3.33 mm at 1 mm, with an average deviation of 13.6% between methods.

rnational Journal Of Innovative Trends In Multi Disciplinary Scientific Research
ISSN (Online): 3139 – 2687
(www.ijtmsr.co.in) Volume 9, Issue 8, 2026

Graphite Epoxy

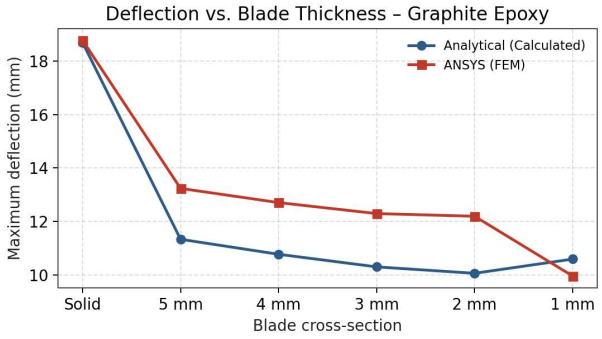


Fig 16 Deflection versus blade thickness, Graphite Epoxy.

ANSYS deflection falls to a minimum of 9.97 mm at 1 mm (46.9% reduction); the analytical minimum of 10.070 mm occurs at 2 mm before rising to 10.60 mm at 1 mm, with an average deviation of 13.6% between methods.

Bending Stress Results – Aluminum

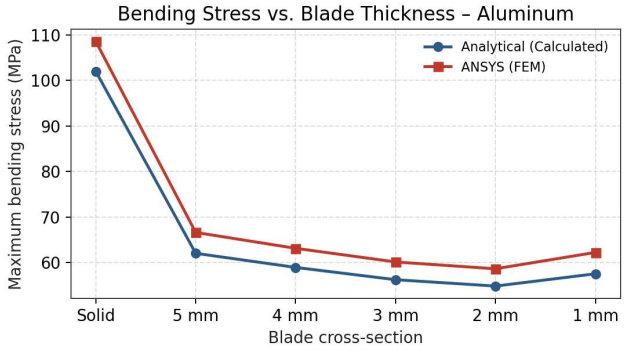


Fig 17 Bending stress versus blade thickness, Aluminum.

Bending stress follows the same trend as deflection: the solid Aluminum blade shows the highest stress (ANSYS 108.6 MPa vs. analytical 102 MPa) at the supports, falling to a minimum ANSYS value of 58.60 MPa at 2 mm before rising again at 1 mm. The average deviation between methods is 7.2%, supporting use of the analytical formulae for the remaining materials, for which full FEM stress results were not separately tabulated.

B. MODAL ANALYSIS RESULTS

The modal analysis evaluates the first three natural frequencies (f_1, f_2, f_3) of each blade configuration, obtained both analytically and from the ANSYS eigenvalue solution. Table 4.7 to Table 4.12 and Figures 4.7–4.12 present these results for each material across all six cross-sections. For all six materials, the three natural frequencies generally increase as the wall is thinned, since mass reduction outweighs the loss of bending stiffness over most of the range — a trend consistent, though not perfectly monotonic at every intermediate thickness, and expected from beam vibration theory. Analytical and ANSYS results track closely, with average deviations of roughly 5–9% across the three modes for each material; ANSYS values run consistently slightly higher, typical when comparing a full three-dimensional FEM model against a simplified beam formulation.

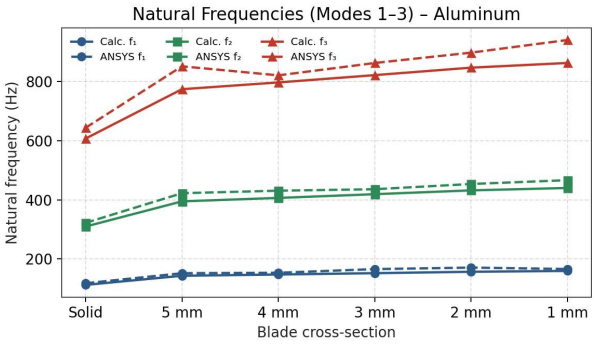


Fig 18 First three natural frequencies versus blade thickness, Aluminum.

ANSYS f_1 rises from 117.9 Hz (solid) to 166.0 Hz at 1 mm (40.7%); f_3 rises from 643.5 Hz to 940.2 Hz (46.1%). Average deviations: f_1 6.2%, f_2 5.3%, f_3 6.5%.

Kevlar 149 Natural frequency

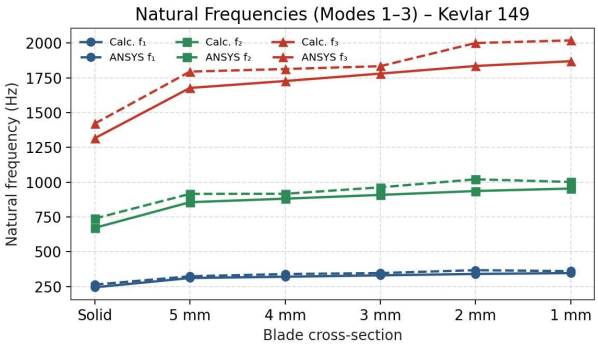


Fig 19 First three natural frequencies versus blade thickness, Kevlar 149.

ANSYS f_1 rises from 262.9 Hz (solid) to 359.7 Hz at 1 mm (36.8%); f_3 rises from 1420.8 Hz to 2019.0 Hz (42.1%). Average deviations: f_1 5.8%, f_2 6.8%, f_3 6.7%.

Technora Natural frequency

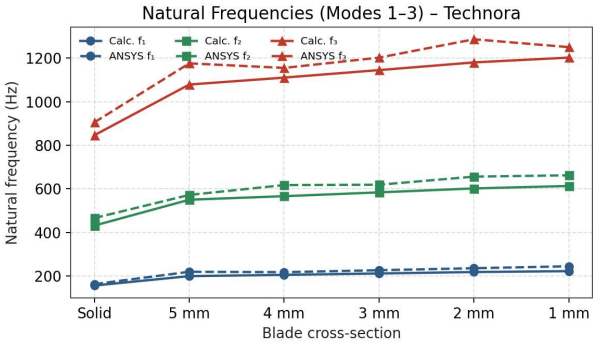


Fig 20 First three natural frequencies versus blade thickness, Technora.

ANSYS f_1 rises from 162.8 Hz (solid) to 244.7 Hz at 1 mm (50.3%); f_3 rises from 905.3 Hz to 1250.3 Hz (38.1%). Average deviations: f_1 7.5%, f_2 7.3%, f_3 6.3%.

rnational Journal Of Innovative Trends In Multi Disciplinary Scientific Research
ISSN (Online): 3139 – 2687
(www.ijtmsr.co.in) Volume 9, Issue 8, 2026

Glass E Natural frequency

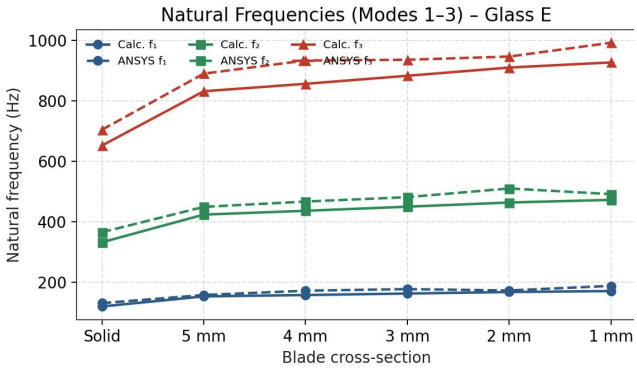


Fig 21 First three natural frequencies versus blade thickness, Glass E.

ANSYS f_1 rises from 131.5 Hz (solid) to 188.6 Hz at 1 mm (43.4%); f_3 rises from 704.3 Hz to 991.6 Hz (40.8%). Average deviations: f_1 7.2%, f_2 7.3%, f_3 6.8%.

Glass S Natural frequency

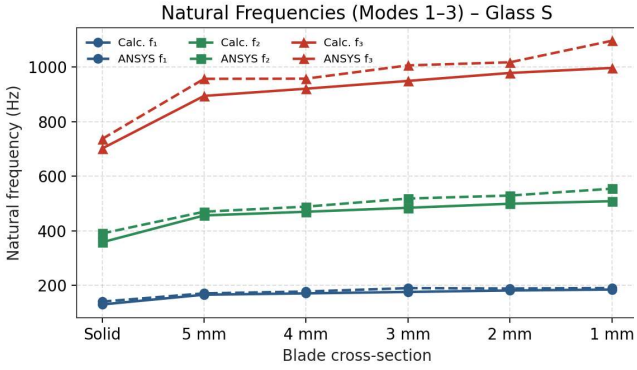


Fig 22 First three natural frequencies versus blade thickness, Glass S.

ANSYS f_1 rises from 140.2 Hz (solid) to 190.1 Hz at 1 mm (35.5%); f_3 rises from 736.8 Hz to 1096.9 Hz (48.9%). Average deviations: f_1 5.0%, f_2 6.3%, f_3 6.0%.

Graphite Epoxy Natural frequency

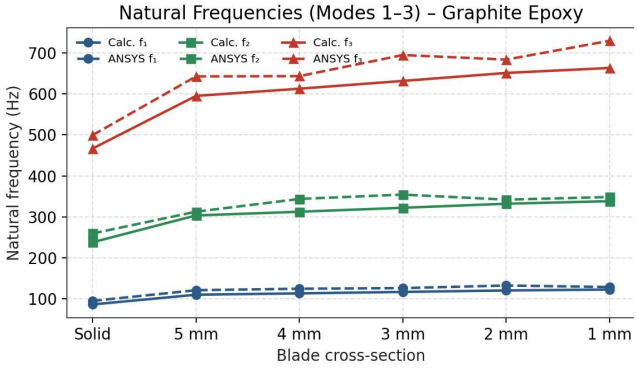


Fig 23 First three natural frequencies versus blade thickness, Graphite Epoxy.

ANSYS f_1 rises from 95.0 Hz (solid) to 128.9 Hz at 1 mm (35.6%); f_3 rises from 499.5 Hz to 729.7 Hz (46.1%). Average deviations: f_1 8.8%, f_2 6.3%, f_3 7.5%.

V. Conclusion

A NACA 0015 straight-bladed VAWT was evaluated using analytical beam theory and ANSYS FEA for six wall thicknesses and six candidate materials. The two methods showed consistent trends for deflection, bending stress and natural frequency. Reducing the solid section to a thin-walled configuration lowered structural loading and improved static response until the loss of section stiffness became important. The analytical results identify approximately 2 mm as the most favorable thickness for minimum deformation and stress, while FEM results show that 1–2 mm sections can remain competitive depending on material. Modal frequencies generally increased with decreasing wall thickness because mass reduction outweighed stiffness loss over most of the range. Kevlar 149 offered the best overall stiffness-to-weight response, with Glass S and Glass E also performing favorably. For practical design, a 2–3 mm high-stiffness composite section is recommended as a balanced starting range, subject to subsequent aerodynamic–structural coupling, composite layup definition, fatigue assessment and experimental validation.

REFERENCES

[1] Seralathan, S., et al. (2020). Static structural analysis of cross flow vertical axis wind turbine. Materials Today: Proceedings, 33, 3630–3639.

[2] Öğüçlü, Ö. (2020). Structural design and stress analysis of a helical vertical axis wind turbine blade. Sakarya University Journal of Science, 24(6), 1151–1161.

[3] Hand, B. P., Kelly, G., & Cashman, A. (2021). Structural analysis of an offshore vertical axis wind turbine composite blade experiencing an extreme wind load. Marine Structures, 75, 102858. https://doi.org/10.1016/j.marstruc.2020.102858

[4] Carnevale, M., et al. (2021). Structural response and fatigue assessment of a small vertical axis wind turbine under stationary and non-stationary excitation. Renewable Energy, 170, 251–266. https://doi.org/10.1016/j.renene.2021.01.123

[5] Nachtane, M., et al. (2022). Numerical investigation of the structural behavior of an innovative offshore floating Darrieus-type wind turbine with three-stage rotors. Journal of Composites Science, 6(6), 167.

[6] Boudounit, H., Tarfaoui, M., & Saifaoui, D. (2023). Fatigue analysis of wind turbine composite blade using finite element method. Wind Engineering, 47(3).

[7] Akimoto, H., et al. (2024). Structural optimization using a genetic algorithm aiming for the minimum mass of vertical axis wind turbines using composite materials. Heliyon, 10, e33185. https://doi.org/10.1016/j.heliyon.2024.e33185

[8] Nezzar, H., Ferroudji, F., & Outtas, T. (2025). Numerical investigation of the structural-response analysis of a glass/epoxy composite blade for small-scale vertical-axis wind turbine. Wind Engineering, 49(1). https://doi.org/10.1177/0309524X241259945

[9] Mishnaevsky, L., et al. (2020). Materials for wind turbine blades: An overview of materials, damage and sustainability developments. Composite-materials literature.

[10] Jensen, F. M., & Branner, K. (2020). Structural design considerations for modern composite wind turbine blades. Wind-turbine structural-design literature.

[11] Lagdani, O., Tarfaoui, M., Nachtane, M., Trihi, M., & Laaouidi, H. (2022). Modal analysis of an iced offshore composite wind turbine blade. Wind Engineering, 46(1).

[12] Jayswal, S., & Bhattu, A. (2023). Structural and modal analysis of small wind turbine blade using three different materials. Materials Today: Proceedings, 72, 1347–1352.

[13] Nijssen, R. P. L., & Brøndsted, P. (2023). Fatigue as a design driver for composite wind turbine blades. In Advances in Wind Turbine Blade Design and Materials (2nd ed.). Elsevier.

[14] Ghoneam, S. M., Hamada, A. K., & Sherif, T. S. (2024). Fatigue-life estimation of vertical-axis wind turbine composite blades using modal analysis. Journal of Energy Resources Technology, 146(3). https://doi.org/10.1115/1.4064178

[15] Hardt, D., et al. (2024). Comparison of different cross-sectional approaches for the structural design and optimization of composite wind turbine blades based on beam models. Wind Energy Science, 9, 1465–1486.